steel research international
www.steel-research.de

Deep Cryogenic Treatment of Various Electrodes for Enhanced Electrochemical Machining Performance of Wire Arc Additive Manufactured Stainless Steel

Karunakaran Kuppusamy, Gopi Periyappillai, Saravanakumar Sengottaiyan, and Periyasamy Rajendran*

This study aimed to evaluate the effect of deep-cryogenic treatment (DCT) on the properties of electrodes, including corrosion resistance, electrochemical stability, and electrochemical machining (ECM) performance, in wire arc-produced SS309. Deposition parameters such as voltage (8, 10, and 12 V), electrolyte concentration (20, 30, and 40 g/l), duty cycle (45, 55, and 65%), and pulse frequencies (40, 50, and 60 Hz) are varied to examine ECM performance. The electrical conductivities of BeCu and SS304 increased by 37.88% and 83.31%, respectively, indicating easier ion transfer and better machining capabilities. The corrosion resistance of DCT-modified electrodes is further improved, with corrosion current densities decreasing by 26.1% for BeCu and 43.5% for SS304. Electrochemical stability tests showed that DCT enhanced the stability of both electrodes, evidenced by a slight shift toward more positive corrosion potentials and lower current responses. In terms of ECM performance, compared to untreated electrodes, DCT-treated samples achieved higher material removal rates, improved circularity, and reduced conicity, indicating better geometric accuracy and surface quality. DCT-treated SS304 electrodes exhibited the best performance, with increased machining stability and precision. This research demonstrates that DCT is a promising method for improving the ECM process, especially in high-precision fields such as aerospace, automotive, and biomedical manufacturing.

1. Introduction

One unconventional method for shaping complex forms with tight tolerances in difficult-to-machine materials, such as high-strength steels, alloys, and composites, is the process known as electrochemical machining (ECM).[1–3] This technique is particularly beneficial for high-hardness materials like stainless steel because it eliminates thermal and mechanical stresses often caused by traditional machining methods like grinding or milling.[4–6] However, ECM encounters specific challenges when working with steel and stainless steel.[7–9] These challenges must be managed while ensuring high precision, reducing tool wear, and achieving a quality surface finish.[10–12] Since the tool electrode erosion is significant due to electrochemical dissolution in conventional processes, processing efficiency drops, and accuracy suffers.[13,14] Moreover, issues such as electrode corrosion and electrochemical instability can result in inconsistent machining, especially with high-strength steels like SS304.[15,16] Additionally, using nonprepared electrodes often leads to side-tool wear and overcutting, which cause geometric inaccuracies and surface damage.[17]

Recently, there has been increased interest in cryogenic treatment to improve the performance of ECM electrodes. This process involves cooling the electrodes to cryogenic temperatures, usually with liquid nitrogen, resulting in a finer microstructure.[18] Grain structure refinement, reduction of residual stress, and uniform dispersion of carbide enhance their hardness, wear resistance, and electrochemical stability.[19,20] Cryo-treated electrodes demonstrate improved corrosion resistance and excellent electrical conductivity, leading to more uniform electrochemical reactions and less tool wear during ECM. Consequently, this boosts machining productivity, increases the material removal

K. Kuppusamy
Department of Mechanical Engineering
Vels Institute of Science Technology and Advanced Studies (VISTAS)
Chennai 600117, India

G. Periyappillai
Department of Automobile Engineering
Easwari Engineering College
Chennai 600089, India

The ORCID identification number(s) for the author(s) of this article can be found under https://doi.org/10.1002/srin.202501127.

DOI: 10.1002/srin.202501127

S. Sengottaiyan
Faculty of Engineering and Technology
Villa College
Male 20373, Maldives
E-mail: s.sengottaiyan@villacollege.edu.mv

P. Rajendran
Department of Mechanical Engineering
Kongunadu College of Engineering and Technology
Tiruchirappalli, Tamil Nadu 621215, India

rate (MRR), and improves the part's dimensional accuracy.[21,22] Wire arc additive manufacturing (WAAM) is an emerging method for producing steel and alloy parts through additive processes.[23,24] It provides advantages over traditional techniques like material removal or casting, especially for creating complex-shaped parts with high strength and good mechanical properties.[25] However, machining WAAM-enhanced materials is challenging due to inherent residual stresses, anisotropic microstructure, and fracture characteristics.[26] These features make machining WAAM materials such as SS309 difficult, but ECM enables precise surface deposits without adding extra mechanical or thermal stress.[27] For future applications in corrugated board production, it is crucial to understand the interaction between ECM and various WAAM materials to select appropriate electrode materials that address limitations and improve surface quality.[28]

In this study, BeCu and SS304 are examined as two commonly used electrode materials. BeCu has been increasingly used in ECM, mainly because its excellent electrical conductivity combines with high toughness, which resists wear.[29,30] It is also known for its electrochemical stability across different working environments.[31] SS304, an austenitic stainless steel, offers excellent corrosion resistance and mechanical properties, making it an ideal material for ECM requiring high precision and abrasion resistance.[32] However, both materials have drawbacks such as side erosion, tool wear, and low surface roughness in ECM, issues that can potentially be mitigated through cryogenic treatment.[33,34] This work aims to investigate the tribology and heat effects of cryogenically treated BeCu and SS304 electrodes in the ECM of WAAM-deposited SS309 material. Specifically, the research assesses how cryogenic treatment impacts conductivity, corrosion resistance, MRR, and the effects on circularity and conicity. The findings contribute to a better understanding of how cryogenic treatment influences tool wear, accuracy, and machining efficiency during ECM for WAAM SS309, which is considered a strengthening process. For stainless steels and machine-resistant alloys, significant interest exists in electrochemical micromachining (ECMM), including electrolyte development, tool electrode design, and process parameter control. Please refer to **Table 1** for the literature overview.

Despite the extensive literature on ECM, only a few studies focus on electrolyte composition, process parameters such as voltage, duty cycle, and frequency, or electrode geometry. These studies have greatly enhanced machining efficiency and MRR, and reduced defects like overcut and taper. However, a significant gap in the literature is the lack of emphasis on modifying the electrode material properties themselves, which directly influence electrochemical stability, conductivity, corrosion resistance, and dimensional accuracy during ECM. Additionally, while stainless steels such as SS304 have been widely examined, there is limited research on WAAM-fabricated stainless steels like SS309, which present unique challenges due to their heterogeneous microstructure and residual stresses.

Table 1. Literature summary for existing studies on ECM.

Author and year	Material/ electrode	Focus parameters	Key findings	Gap identified/contribution
Ben Mhahe et al.[53]	Molybdenum/ Brass	Electrolyte type and conc.	Mixed alkaline/neutral electrolytes improved MRR and surface integrity	Did not consider electrode treatment
Mouliprasanth and Hariharan[55]	SS304/Cu	Electrolyte comparison	Composite electrolytes improved MRR, circularity & conicity	Focused only on electrolyte effects
Thangamani et al.[56]	SS304/Cu	NaCl-based electrolytes	Tamarind + NaCl improved MRR (+29%) and reduced overcut (−47%)	No electrode modification studied
Pradeep et al.[57]	SS304/Polymer graphite	$NaNO_3$ electrolyte	Voltage contributed ≈52% to MRR and taper; duty cycle is also critical	Limited to polymer electrodes
Min Soo Park and Chu[58]	MicroECM, multiple electrodes	Tool design and pulse control	Multiple tool electrodes improved machining efficiency and hole accuracy	Did not evaluate electrode metallurgy or treatments
Zhu et al.[59]	SS304/Graphite	Microhole machining, pulse frequency	Hollow graphite electrode reduced clogging; optimized frequency and voltage reduced taper to 0.07	Focused on electrode geometry, not treatment
Kumar et al.[60]	Alloys and MMCs/Various electrodes	ECMM reviews & optimizations	Mixed electrolytes and pulse rectifier design improved accuracy and surface quality.	Review study; did not address cryogenic treatment.
Engin Nas and Nursel Altan Ozbek[61]	Hardened Hot Work Tool Steel	Turning of hardened tool steel	DCT improves surface finish, tool wear, and dimensional accuracy, especially in hard-to-machine materials like hardened tool steel.	Focused on turning; did not address ECM or electrode materials.
Engin Nas[62]	AISI H13 Hot Work Tool Steel	Cryogenic treatment, EDM performance	Cryogenic treatment improved surface roughness, wear resistance, and machining precision. The study emphasizes the statistical analysis of EDM performance postDCT.	Investigates the effects of cryogenic treatment on electrode wear, surface finish, and crater formation in EDM.
Present study	WAAM SS309/ BeCu & SS304 (NCT vs. DCT)	Electrical conductivity, corrosion resistance, MRR, circularity, conicity, SEM	DCT improved conductivity, corrosion resistance, and machining accuracy; SS304-DCT performed best	First to integrate cryogenic treatment with BeCu and SS304 electrodes for ECM of WAAM steels.

This study addresses a research gap by systematically exploring how DCT influences BeCu and SS304 electrodes in the ECM of WAAM SS309 material. Unlike standard parameter or electrolyte optimization, the innovation lies in altering the electrode microstructure through cryogenic treatment to refine grains, reduce residual stresses, and improve carbide uniformity. These structural modifications notably enhance electrode conductivity, corrosion resistance, and electrochemical stability, leading to improved machining performance. The study's novelty is twofold: first, it is among the pioneers to investigate cryogenically treated electrodes in the ECM of WAAM materials, bridging additive manufacturing and precision machining; second, it offers a comparative analysis of BeCu and SS304 electrodes under NCT and DCT conditions, with SS304-DCT delivering the best results for high MRR, reduced circularity error, and minimal conicity. Overall, this research uniquely combines cryogenic treatment with ECM electrode preparation, demonstrating that electrode modification is as important as electrolyte or parameter optimization in enhancing machining accuracy and surface quality of advanced additively manufactured materials.

2. Experimental Section

2.1. Materials and Workpiece Preparation

WAAM-fabricated austenitic stainless steel SS309, produced in the prior work (**Figure 1**a),[35] was used as the anode (workpiece) for all ECMM trials. The fine surface of the WAAM-fabricated SS309 wall prepared for sample extraction is shown in Figure 1b. The corresponding etched microstructure of the WAAM SS309, revealing the austenite–δ-ferrite morphology characteristic of layer-wise thermal cycling, is provided in Figure 1c. Rectangular coupons were extracted from the WAAM walls by wire-EDM to the required size (e.g., 10×10 mm; thickness as deposited), lightly deburred, ultrasonically cleaned in ethanol, and oven-dried at 60 °C. The as-deposited chemistry of the WAAM SS309 was confirmed from EDX measurements and used as a reference for discussion, without further alloy modification in the present work.[35]

Tool pins and needles were prepared with identical geometries for fair comparison (length ≈30 mm; tip diameter chosen to achieve the target feature size). The chemical composition of the electrodes used in this study, BeCu and SS304, is listed in **Table 2** and **3**. Before any treatment, tools were progressively polished using SiC papers (P320–P4000), followed by a 0.05 µm alumina slurry to create a mirror finish. They were then degreased in acetone, rinsed with deionized (DI) water, and dried with nitrogen. For each material, matched batches of noncryogenically treated (NCT) and deep-cryogenically treated (DCT) tools were prepared from BeCu to isolate the effect of cryogenic treatment. The electrolyte was a neutral salt mixture of NaCl and $NaNO_3$ (1:1 by weight), prepared in DI water at concentrations of 20, 30, and 40 g L^{-1}. Fresh electrolyte was used for each experimental batch. Bulk conductivity and pH were recorded before use and after each batch to ensure stability.

2.2. DCT of Tools

Cryogenic treatment of SS304 and BeCu tools followed a three-stage cool–soak–warm protocol aimed at microstructural refinement and stress relaxation (**Figure 2**). After precleaning (Section 2.1), the tools were placed in a ventilated copper holder

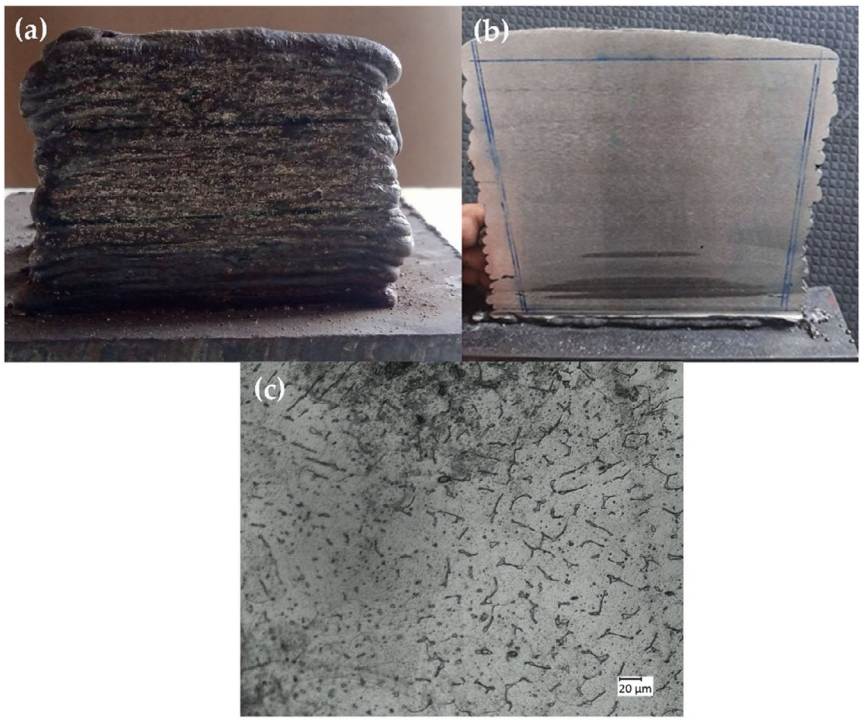

Figure 1. a) WAAM-fabricated SS309 wall,[35] b) fine surface of the wall ready to cut out samples, and c) optical microscope image after etching.

Table 2. Chemical composition of BeCu.[29,31]

Element	Cu	Be	Co
Chemical composition [wt%]	97.9	1.9	0.2

Table 3. Chemical composition of SS304.

Element	C	Cr	Ni	Mo	Mn	Si	P	S	Cu	Fe
Chemical Composition [wt%]	0.017	18.0	8.0	0.40	1.79	0.37	0.03	0.01	0.34	71.04

and ramped from room temperature (≈25 °C)−−196 °C (liquid nitrogen) over ≈180 min to avoid thermal shock. A 24 h soak at −196 °C was maintained, based on prior studies (Ji et al.;[36] Arumugam et al.[37]), to achieve optimal transformation and microstructural equilibration. After the soaking period, the tools were slowly returned to room temperature over ≈3 h in still air. No tempering was applied to isolate the effects of deep-cryogenic exposure. The treated tools were then stored in desiccators before testing and machining. Parallel NCT tools from the same batch were used as controls.

2.3. Electrode Characterization: Conductivity, Corrosion, and Microscopy

To establish the property changes imparted by DCT, tools were characterized before and after treatment. 1) Electrical conductivity/resistivity; Axial resistivity was measured at room temperature using a calibrated LCR/four-terminal setup. For each tool type and condition (SS304-NCT, SS304-DCT, BeCu-NCT, BeCu-DCT), $n = 5$ repeated measurements were taken at an identical gauge length. Electrical conductivity (σ) was computed from $\sigma = L/(\mathrm{RA})$, where L is the gauge length, A the cross-sectional area, and R the measured resistance. Mean ± SD are reported; outliers identified by Grubbs' test ($\alpha = 0.05$) were discarded; 2) corrosion behavior; Potentiodynamic polarization tests were conducted in aerated 3.5 wt% NaCl at 25 ± 2 °C using a three-electrode cell with the tool as working electrode (exposed area precisely masked), a saturated calomel (or Ag/AgCl) reference, and a platinum counter electrode. After 30 min open-circuit potential stabilization, scans were performed at ≈1 mV s^{-1} around OCP. Corrosion potential (E_corr), corrosion current density (i_corr), and Tafel slopes were obtained by standard extrapolation to compare NCT vs. DCT trends for SS304 and BeCu; and 3) optical/scanning electron microscope (SEM)-energy dispersive x-ray spectroscopy (EDX) of tool tips; Tool tips were inspected optically (bright-field) for edge integrity and surface finish. High-resolution SEM imaging and EDX mapping/spot analysis were used 1) preECMM to confirm polishing quality and any DCT-induced surface features and 2) postECMM to assess wear, passivation products, pitting, or salt deposits. Samples were gently rinsed in DI water and ethanol, dried, and sputter-coated (if required for charge mitigation) before SEM.

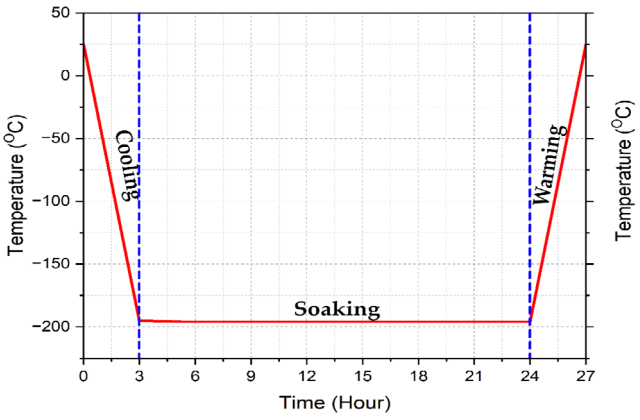

Figure 2. DCT process.

2.4. ECM Setup

ECM experiments were performed on a custom microECM test bed with independent control of applied voltage (8, 10, 12 V), pulse duty cycle (45, 55, 65%), pulse frequency (40, 50, 60 Hz), and electrolyte concentration (20, 30, 40 g L^{-1}). The workpiece (WAAM SS309) was positively biased (anode), and the tool was negatively biased (cathode). Electrolyte (NaNO3) was delivered through a chemically resistant manifold to the interelectrode gap at a constant flow rate and temperature, which was monitored during each run. The stepper motor used in our setup has the following specifications: 60 steps per revolution (6° per step), a minimum rotation angle of 6° per step, and voltage ratings of 8, 10, and 12 V, which were used to control voltage during the experiments. The motor's current rating is 1.2 A, and the model is NEMA 23a. These specifications enable precise control of the electrode movement along the Z-axis during the ECM process. The minimum linear displacement of the lead/ball screw in the Z-axis per single pulse is calculated using the following formula (1).[38]

$$\begin{aligned}&\text{Linear Displacement per pulse}\\ &= \frac{\text{Motor rotation per pulse}}{360^\circ} \times \text{lead of the screw}\\ &= \frac{6^\circ}{360^\circ} \times 2 = 0.0333\,\text{mm}\end{aligned} \tag{1}$$

Voltage pulsing was generated by a programmable DC source with an external pulse-train controller; the waveform was verified on an oscilloscope before machining. All trials used identical mechanical alignment and flushing conditions. Each experimental condition was performed for both tool materials (SS304, BeCu) and treatments. To minimize drift, the run order was randomized, and the electrolyte was refreshed between blocks.

2.5. Design of Experiments and Replication

The study consisted of three integrated phases without optimization or inferential statistics. First, SS304 and BeCu tools were divided into noncryogenic (NCT) and deep-cryogenic (DCT) lots and characterized for electrical conductivity, corrosion behavior (potentiodynamic polarization), and surface condition

(optical/SEM-EDX). Second, ECMM of WAAM SS309 was conducted using a nine-run, orthogonally balanced matrix with voltage levels of 8/10/12 V, electrolyte concentrations of 20/3/40 g L^{-1}, duty cycles of 45/55/65%, and frequencies of 40/50/60 Hz; the same nine settings were applied independently to SS304-NCT/DCT and BeCu-NCT/DCT in randomized order, keeping gap, tool geometry, flow, and temperature constant. Each condition was tested in triplicate and reported as mean ± SD for MRR, circularity error, and conicity.

2.6. Response Measurements: MRR, Circularity, and Conicity

MRR was measured gravimetrically using a 0.1 mg balance. Parts were degreased, rinsed, and dried before and after machining; $MRR = (M_1 - M_2)/t$, where M_1 and M_2 are the initial and final masses, and t is the machining time.[39,40] Reported MRR values are the average of three repeats with standard deviation. Circularity error of the machined microfeatures (through-holes/bores) was quantified from plan-view images captured with a calibrated toolmaker's microscope/vision system. A least-squares circle fit was applied to the extracted edge; circularity error was calculated as the radial deviation between the maximum inscribed and minimum circumscribed circles (or the equivalent ISO definition used by the lab). Conicity was determined from the entrance (D_ent) and exit (D_ex) diameters measured by optical microscopy/3D profilometry on sectioned samples: $Conicity = (D\_ent - D\_ex)/2h$, where h is the local depth. Positive values indicate taper narrowing along the machining direction. Measurement uncertainty was assessed from repeated measurements (at least three locations per hole).

2.7. SEM Analysis of Machined Surfaces

Selected holes machined with SS304-NCT, SS304-DCT, BeCu-NCT, and BeCu-DCT at representative parameter sets were sectioned, rinsed to remove salt residues, and gently dried. SEM (using secondary and backscattered modes) was used to evaluate surface morphology, recast/passivation layers, striations, pitting, and sludge buildup. When needed, EDX was employed to identify metallic dissolution products (Fe/Cr/Ni for SS309; Cu/Be for BeCu transfer) and chloride/nitrate residues from the electrolyte.

3. Results and Discussion

3.1. Microstructure of Base Metal (WAAM-Fabricated SS309)

SEM of the WAAM SS309 base metal shows (**Figure 3**a) a duplex austenitic matrix with skeletal or vermicular δ-ferrite decorating austenite grains and interdendritic regions, giving the surface a discontinuous, slot-like morphology. EDS (Figure 3b) from the same field (Fe ≈ 61.6, Cr ≈ 24.8, Ni ≈ 13.3, Mo ≈ 0.25 wt%) confirms Fe—Cr—Ni as the principal constituents with minor Mo, typical of 309-grade stainless, and aligns with reports that both δ-ferrite and γ-austenite contain Cr, Fe, and Ni, with Cr enrichment near δ/γ boundaries and slight Ni enrichment in the γ matrix. This study's observations also concur with the literature describing WAAM SS309L as mainly FCC γ-austenite with BCC δ-ferrite, where δ-ferrite resides along austenite boundaries.

The etched morphology shows columnar, dendritic solidification caused by high thermal gradients in WAAM, which results in γ dendrites with interspersed δ-ferrite and layer-by-layer heterogeneity. Madesh R et al.[41] also revealed columnar γ grains aligned with heat flow and features of δ-ferrite, confirming this microstructural interpretation for the base metal. Overall, the duplex $\gamma + \delta$ morphology and the Fe—Cr—Ni(+Mo) EDS signature we measured closely match the established WAAM SS309L microstructure and elemental distribution, supporting the suitability of our deposited base metal for future ECM trials.

3.2. Electrical Conductivity Test

The electrical conductivity of Beryllium Copper (BeCu) and Stainless Steel (SS304) electrodes was measured both before and after cryogenic treatment (DCT), with results shown in **Table 4**. For BeCu, the conductivity increased from 0.0045611 to 0.007342 S m^{-1}, reflecting a 37.88% increase. In contrast, SS304 demonstrated a much larger improvement, with conductivity rising from 0.1283 to 0.7688 S m^{-1}, an increase of 83.31%.

This significant boost in conductivity, especially for SS304, results from the refinement of the microstructure during DCT. It encourages a more uniform distribution of carbides and reduces dislocations, which enhances electron flow. The notable rise in SS304's conductivity aligns with previous research that observed similar improvements in electrical properties

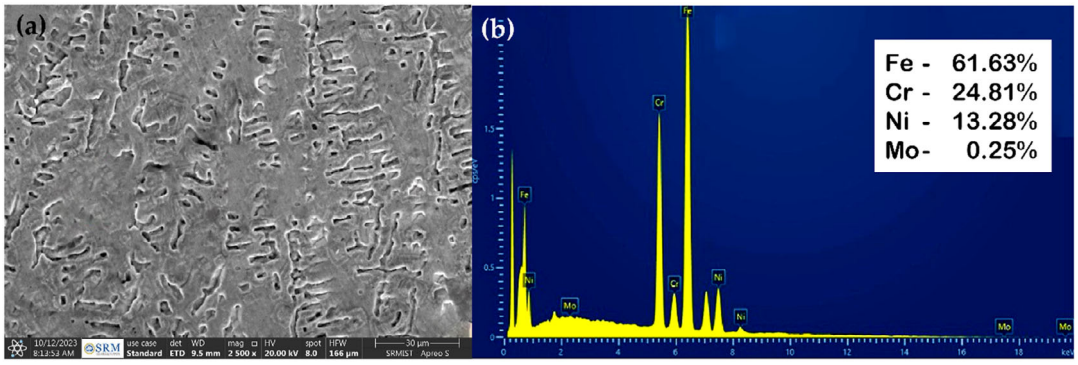

Figure 3. a) SEM image of WAAM SS309 and b) EDS analysis.

Table 4. Electrical conductivity results of the electrode before and after treatment.

Electrodes	Before DCT [S m^{-1}]	After DCT [S m^{-1}]	Percentage variation [%]
Beryllium copper (BeCu)	0.0045611	0.007342	37.877
Stainless steel (SS304)	0.1283	0.7688	83.31

following cryogenic treatment. This enhancement improves the performance of electrodes in electrochemical applications.

3.3. Corrosion Test Analysis

The corrosion resistance of both BeCu and SS304 electrodes before and after DCT was assessed using potentiodynamic polarization tests. The polarization curves for BeCu and SS304 electrodes are shown in **Figure 4**, while **Table 5** lists the corrosion parameters such as anodic onset potential (Ecorr), corrosion current density (Icorr), and polarization resistance (Rp). The results demonstrate that DCT significantly improves the corrosion resistance of both electrode materials by increasing the forward corrosion potential and decreasing the forward anodic current density.

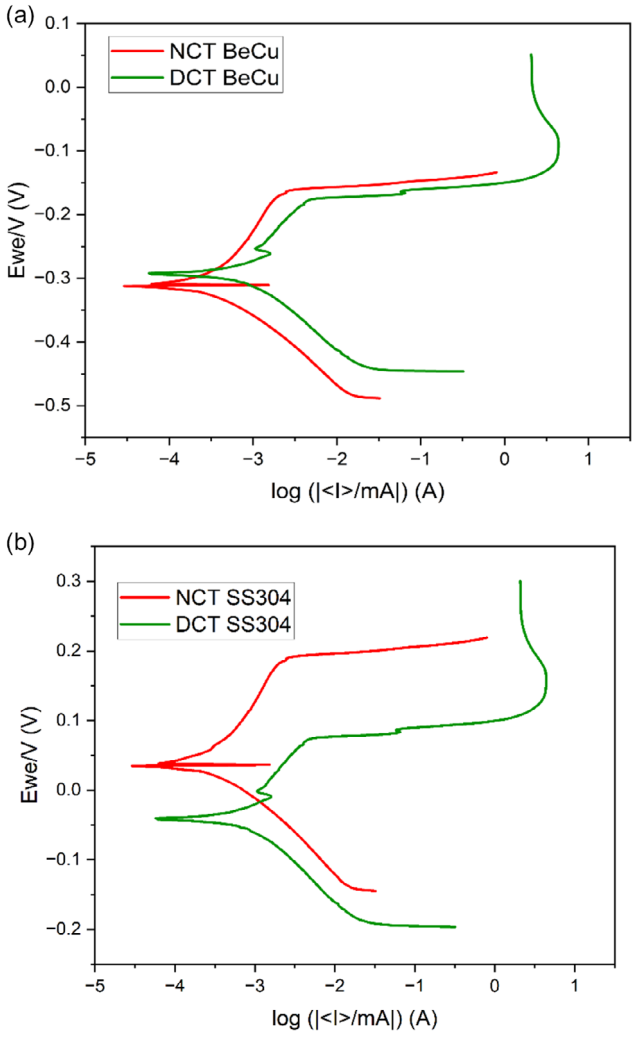

Figure 4. Potentiodynamic polarization curve a) BeCu and b) SS304 electrode.

Table 5. Corrosion test result and electrical stability of electrodes before and after treatment.

Electrodes	Before DCT		After DCT	
	Corrosion resistance [mmpy]	Electrochemical stability	Corrosion resistance [mmpy]	Electrochemical stability
BeCu	0.1513	Less	0.510×10^{-3}	Moderate
SS304	0.0170	Moderate	0.7688	High

Regarding the BeCu electrode (Figure 4a), the untreated sample had an Icorr value of ≈0.092 μA cm^2, which decreased to around 0.068 μA cm^2 after DCT treatment, representing a 26.1% reduction. The Ecorr of the hydrophilic coating (−0.420 V) increased to −0.370 V after DCT, indicating improved corrosion resistance of the electrode. The polarization resistance (Rp) also increased after DCT, corresponding with higher corrosion resistance. These findings align with the study by Voglar et al.,[42] which demonstrated microstructure refinement in high-speed steels and other alloys by promoting uniform carbide precipitation under cryogenic conditions. This process also enhances corrosion resistance by reducing sensitivity to pitting and localized corrosion. As a result, a more stable and continuous passive oxide layer forms on the electrode surface, making it less susceptible to corrosion. Furthermore, cryogenic treatment can decrease the volume of retained austenite and refine the grain structure, which has been shown to improve the electrochemical stability of metals. This effect is especially significant for BeCu, which is often used in applications requiring high wear resistance and corrosion stability.

For the SS304 electrode (Figure 4b), similar improvements occurred after DCT. The untreated SS304 electrode had an Icorr of 0.062 μA cm^2, which dropped to 0.035 μA cm^2 following cryogenic treatment, signifying a 43.5% decrease in corrosion rate. The Ecorr shifted from −0.290 V (untreated) to −0.220 V (DCT), further confirming improved electrochemical stability. The polarization resistance (Rp) of SS304 also increased notably after DCT, indicating a general enhancement in corrosion resistance. These results agree with existing literature, where DCT has been shown to enhance the corrosion resistance of stainless steels by refining the microstructure and reducing corrosion products like green rust. The volume fraction of retained austenite in the microstructure decreases with DCT, which is known to negatively impact corrosion resistance.[43] During cryogenic treatment, retained austenite converts into martensite, forming a uniform microstructure and reducing the risk of localized attack. Additionally, the precipitation of fine, homogeneous carbides in the SS304 electrode during cryogenic treatment helps develop a denser, more stable passive film on its surface, resulting in higher corrosion resistance. Ramesh et al.[44] also observed that cryogenic exposure improves steel corrosion resistance by rearranging nitrides and carbides, increasing uniformity and

passivation capacity, and strengthening passive defense to block corrosive substances. Overall, the corrosion test results show that cryogenic treatment of BeCu and SS304 electrodes enhances their anticorrosion properties. This aligns with other studies demonstrating that cryogenic treatment refines metal microstructure and relieves residual stresses, leading to a stable passive film and better corrosion resistance. However, the degree of improvement varies depending on the material, with SS304 showing a stronger enhancement due to its austenitic phase and greater microstructural response to cryogenic treatment.

3.4. Electrochemical Stability Test

The electrochemical stability of the BeCu and SS304 electrodes before and after DCT was evaluated using cyclic voltammetry. **Figure 5**a displays the voltammogram for the BeCu electrode, where the NCT shows a significant current response, indicating a higher susceptibility to corrosion. After cryogenic treatment, the BeCu electrode exhibits a more subdued current response, suggesting improved electrochemical stability. This aligns with the results in Table 4, where the corrosion resistance for BeCu increased from $0.1513\,\mathrm{mm\,year^{-1}}$ to $0.510\times10^{-3}\,\mathrm{mm\,year^{-1}}$ after DCT, reflecting a change from "less" to "moderate" electrochemical stability.

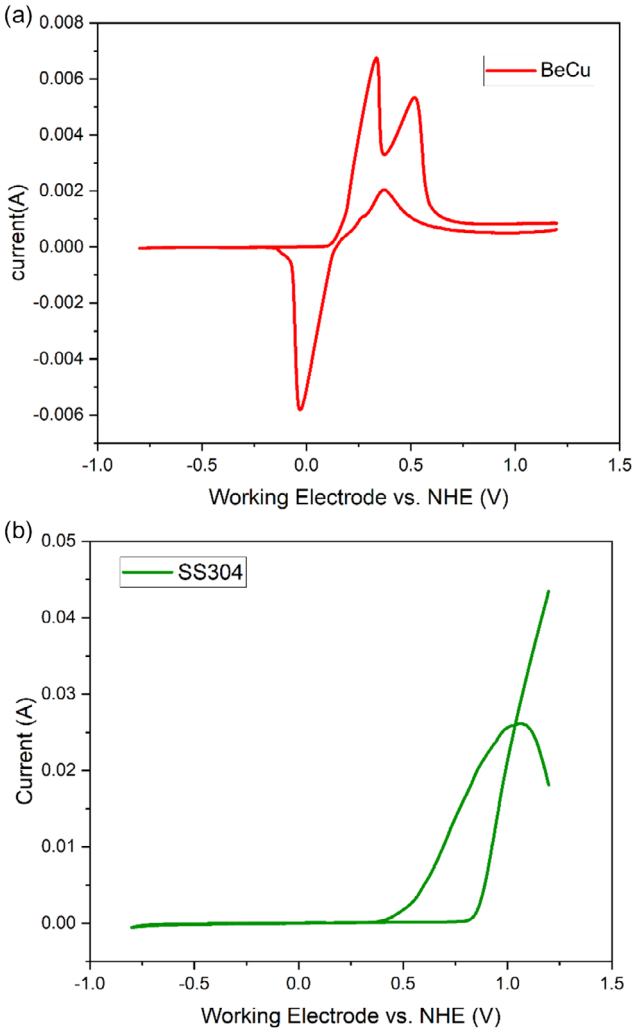

Figure 5. Electrical stability result after DCT a) BeCu and b) SS304 electrodes.

In contrast, for the SS304 electrode (Figure 5b), the untreated electrode displayed a mild current response, typical for stainless steels, with a less prominent peak. After DCT, SS304 showed a sharp increase in current at higher potentials, indicating improved electrochemical stability. This sharper current response suggests that the DCT treatment helped form a more stable passive oxide layer, boosting the material's ability to maintain consistent electrochemical behavior even at higher potentials. As shown in Table 5, the corrosion resistance of SS304 significantly improved from 0.0170 to 0.7688 mm year^{-1}, shifting from moderate to high electrochemical stability after DCT. These findings are consistent with previous studies, where cryogenic treatment has been shown to refine the microstructure of metallic electrodes, reduce residual stresses, and promote the formation of a more stable and protective oxide layer, thereby enhancing electrochemical stability and corrosion resistance.

3.5. Microstructure Analysis of Electrode Before and After Treatment

3.5.1. BeCu Electrode

Microstructural observation of BeCu electrodes (**Figure 6** and **7**) revealed notable differences in morphology between the NCT and DCT. The untreated BeCu electrode (Figure 6a) showed an uneven and rough surface with visible micropits, likely caused by machining defects and local material punctures. This striation effect led to poorer electrochemical performance, indicated by higher overcut and lower MRR, which reduced machining accuracy. In contrast, Figure 6b displays the surface of the DCT-treated BeCu electrode, which appeared smoother and more uniform. These improvements are based on qualitative observations of the SEM and optical microscope images, suggesting a refinement in grain structure and stabilization of the microstructure achieved through cryogenic treatment. These visual enhancements likely help stabilize electrochemical reactions during ECM, resulting in higher MRR and better machining precision, with reduced overcut and circularity deviations.

These findings align with the work of Voglar et al.,[42] who reported that cryogenic treatment significantly refines the microstructure of electrodes, especially in high-speed steels and copper-based alloys like BeCu. The improved surface finish achieved through DCT helps create more stable electrochemical reactions and enhances machining stability, thereby increasing dimensional accuracy in ECM processes. Similarly, Gill and Singh[45] highlighted the importance of deep-cryogenic treatment (DCT) in refining grain structures and boosting tool performance, noting a direct improvement in surface finish and machining precision. This is further supported by Ramesh et al.,[44] who found that cryogenic treatment results in better passivation and material stability, thus enhancing the overall machining process in ECM applications.

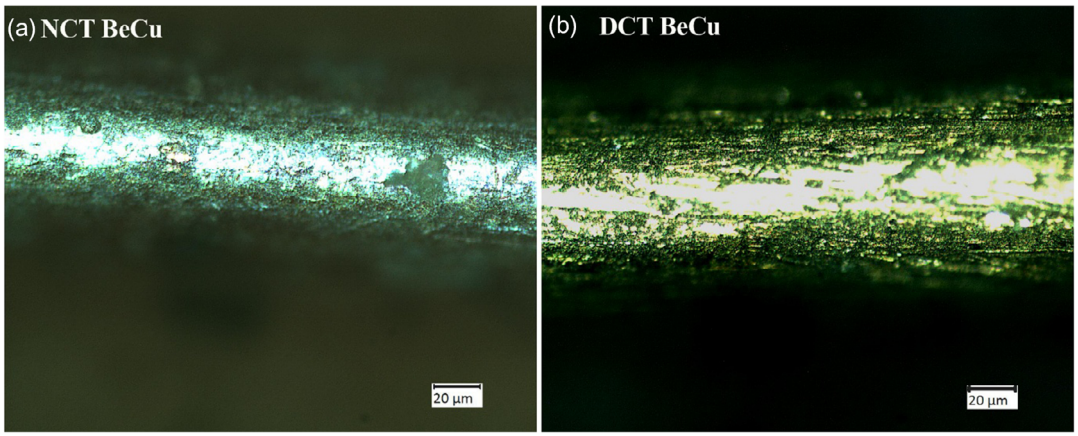

Figure 6. Optical microscope image of BeCu electrode.

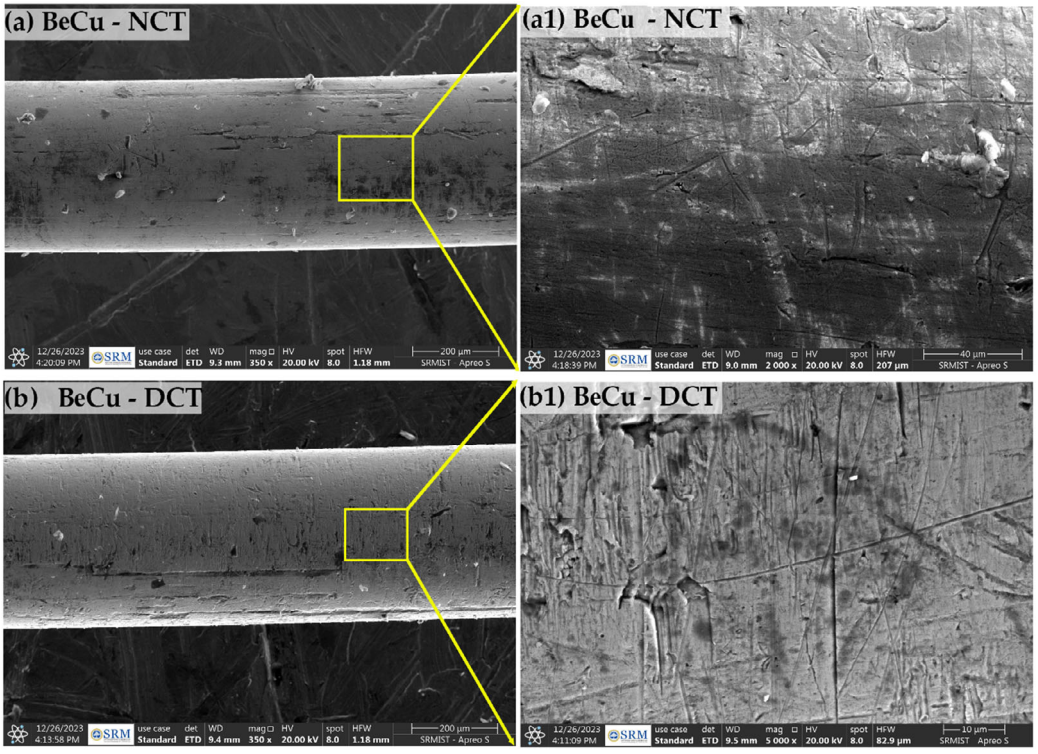

Figure 7. SEM image of BeCu electrode before a,a1) and after treatment b,b1).

SEM imaging of the BeCu electrode (Figure 7a,a1) also supports these interpretation results; DCT-process (Figure 7b,b1) BeCu features homogeneous, smooth grain structures on its surface, which effectively enhance the material properties for ECM. This microstructural improvement corresponds with the significant increase in electrical conductivity after DCT, where conductivity rises by 9.55% for BeCu (Table 4). This enhancement in the contact between the electrode and electrolyte improves ion exchange, resulting in a higher MRR and improved machining accuracy. This aligns with the findings of Sethuraman et al,[37] who observed that cryogenically treated electrodes enhance conductivity, thus directly improving ECM performance. The microscopic and electrochemical improvements observed in the DCT-treated BeCu electrode align with existing literature, confirming that cryogenic treatment effectively enhances the electrochemical stability and cutting performance of BeCu electrodes. Therefore, DCT is a promising treatment method for achieving higher resolution and efficiency in ECM processes, especially in industries where high surface quality and dimensional precision are required.

3.5.2. SS304 Electrode

The microstructure before and after DCT, observed through optical microscopy (**Figure 8**) and SEM analysis (**Figure 9**), showed a clear improvement in surface and microstructural properties due to DCT. The untreated SS304 electrode (Figure 8a) had an uneven surface with microstructural irregularities that could negatively impact electrochemical performance. After DCT (Figure 8b), the surface appeared smoother and more uniform, indicating a refined microstructure. These observations, based on qualitative image analysis, revealed fewer defects and a more stable grain structure, likely contributing to better electrochemical behavior. Cryogenic treatment effectively relieves residual stresses and promotes a more homogeneous grain structure, which enhances electrochemical stability and corrosion resistance.

SEM images of the bare SS304 electrode (Figure 9a,a1) reveal larger, inconsistent grain sizes caused by an uneven morphology with visible surface roughness and wear marks. These features contribute to instability and other issues in ECM, such as MRR and accuracy. In contrast, the DCT-processed SS304 electrode (Figure 9b,b1) shows finer, more uniform grains, fewer surface defects, and improved structural integrity. The microstructure of the DCT-treated electrode suggests that

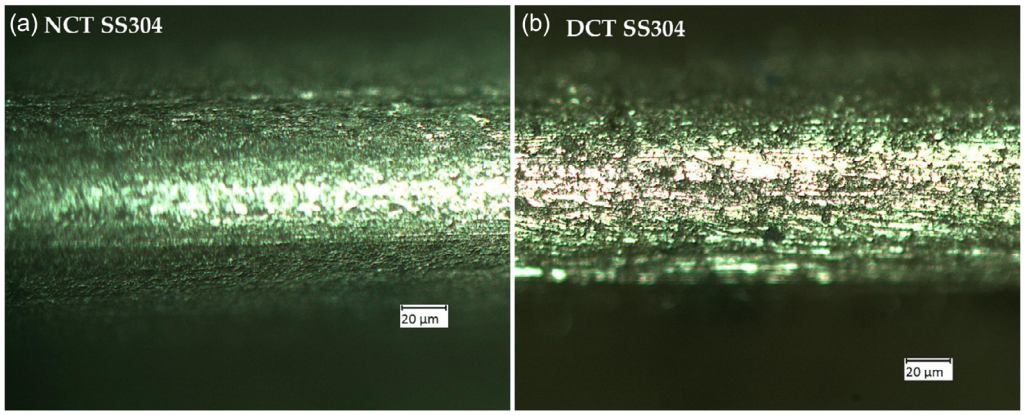

Figure 8. Optical microscope image of SS304 electrode.

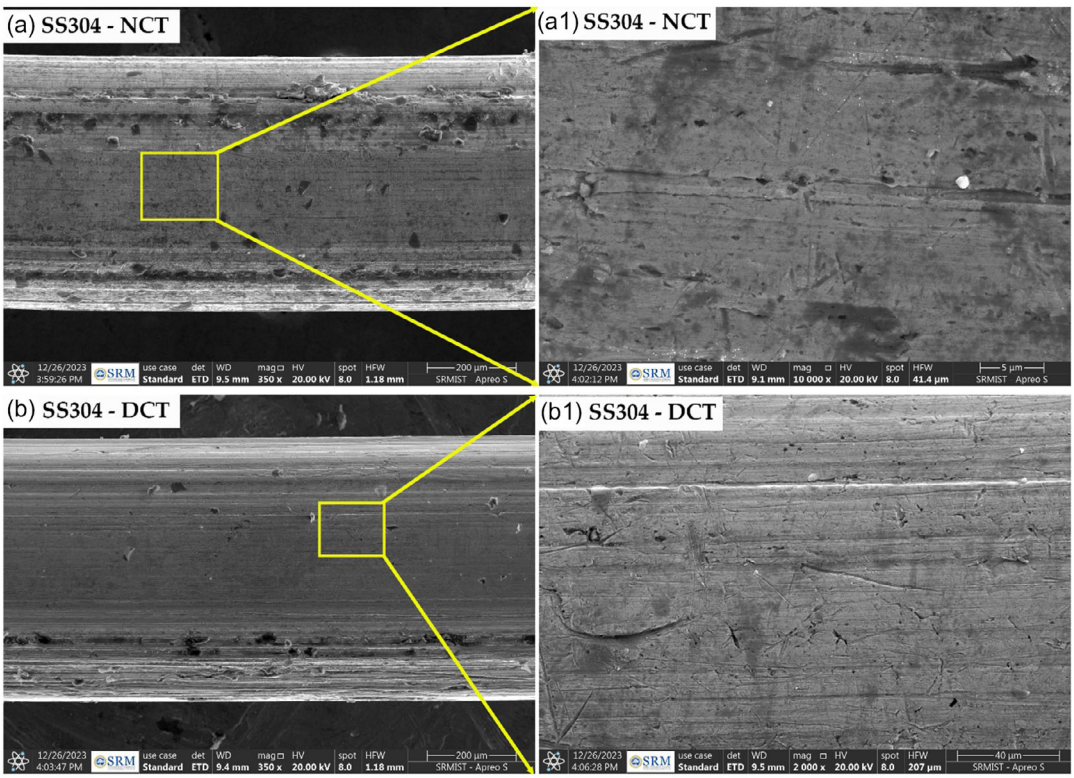

Figure 9. SEM image of SS304 electrode before a,a1) and after treatment b,b1).

cryogenic cooling decreases carbide precipitate size, refines the structure, and boosts surface resistance to wear and corrosion. This reduction in grain size and relief of residual stresses aligns with Voglar et al.,[42] who found that improved surface quality and electrochemical stability of metals following DCT result in overall better machinability.

The enhancement in microstructure after DCT directly correlates with the improved electrochemical performance observed in the corrosion and electrochemical stability tests (Table 4). The microstructure refinement creates a more uniform surface, which promotes more stable electrochemical reactions, lowers corrosion rates, and extends the lifespan of electrodes in industrial applications.[46] Overall, the microstructure of SS304 electrodes after DCT exhibits significant improvements in surface quality and microstructure, making the material more suitable for precise ECM applications. These enhancements align with existing literature, which emphasizes the advantages of cryogenic treatment in refining the material's surface, boosting corrosion resistance, and enhancing electrochemical stability.

3.6. ECM Performance

3.6.1. MRR Behavior of WAAM SS309 Material Using NCT and DCT BeCu and SS304 Electrodes

The MRR and circularity of the machined features exhibited significant improvements after DCT for both BeCu and SS304 electrodes. These improvements can be attributed to the combined effects of enhanced microstructure, improved electrochemical stability, and better electrical conductivity resulting from the DCT process.

For the BeCu electrode (**Figure 10**), a consistent increase in MRR was observed after DCT across most experimental conditions. Specifically, at 8 V, 20 g L^{-1}, 45%, 40 Hz, the MRR for the untreated BeCu (NCT) electrode was 5.40 µg s^{-1}, while the DCT-treated BeCu electrode showed a significant increase to 6.08 µg s^{-1}. Similarly, at 12 V, 40 g L^{-1}, 45%, 40 Hz, the NCT BeCu electrode achieved 8.32 µg s^{-1}, with the DCT-treated BeCu reaching a maximum of 8.56 µg s^{-1}. The increase in MRR is directly linked to microstructure refinement, with DCT reducing surface defects and internal stresses. This improved microstructure enhances the electrode's electrical conductivity, enabling better ion transfer during the ECM process. The enhanced electrochemical stability, resulting from a more stable oxide layer and fewer surface imperfections, leads to more efficient material removal and higher MRR. These findings are consistent with previous research by Jatti et al.,[47] who demonstrated that cryogenic treatment improves ion exchange efficiency and boosts MRR in ECM.

Similarly, for the SS304 electrode (**Figure 11**), the DCT process greatly increased MRR compared to the untreated electrode. At 8 V, 40 g L^{-1}, 65%, 60 Hz, the NCT SS304 electrode had an MRR of 5.28 µg s^{-1}, while the DCT SS304 electrode reached 7.48 µg s^{-1}. At 10 V, 40 g L^{-1}, 65%, 60 Hz, the NCT SS304 electrode achieved 5.9 µg s^{-1}, whereas the DCT-treated SS304 electrode reached a maximum of 8.71 µg s^{-1}. The improvements in MRR for SS304 after DCT are due to a more uniform grain structure and lower residual stresses. The DCT process stabilizes the electrochemical reaction during ECM, resulting in more efficient material removal and higher MRR. This is consistent with the findings of Thangamani et al.,[48] who reported that cryogenic treatment enhances the electrochemical performance of materials, leading to increased MRR.

3.6.2. Circularity Behavior of WAAM SS309 Material Using NCT and DCT BeCu and SS304 Electrodes

The observed improvements in circularity also emphasize the important role of DCT in increasing dimensional accuracy. For the BeCu electrode, the circularity of the machined features was significantly better after DCT. At 10 V, 20 g L^{-1}, 45%, 40 Hz, the untreated BeCu electrode had a circularity of 156.4 µm, while

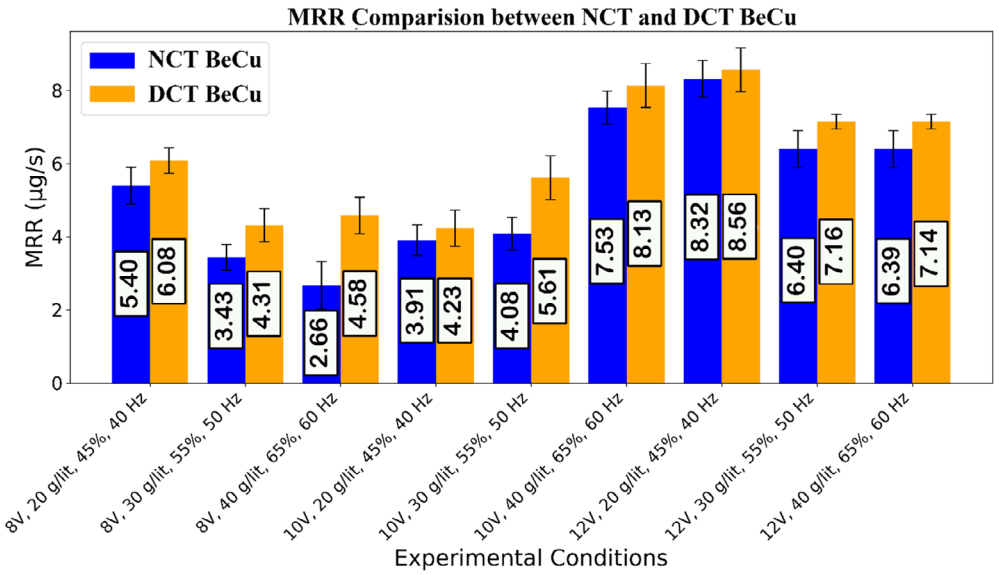

Figure 10. MRR of WAAM SS309 materials using NCT and DCT BeCu electrode during ECM.

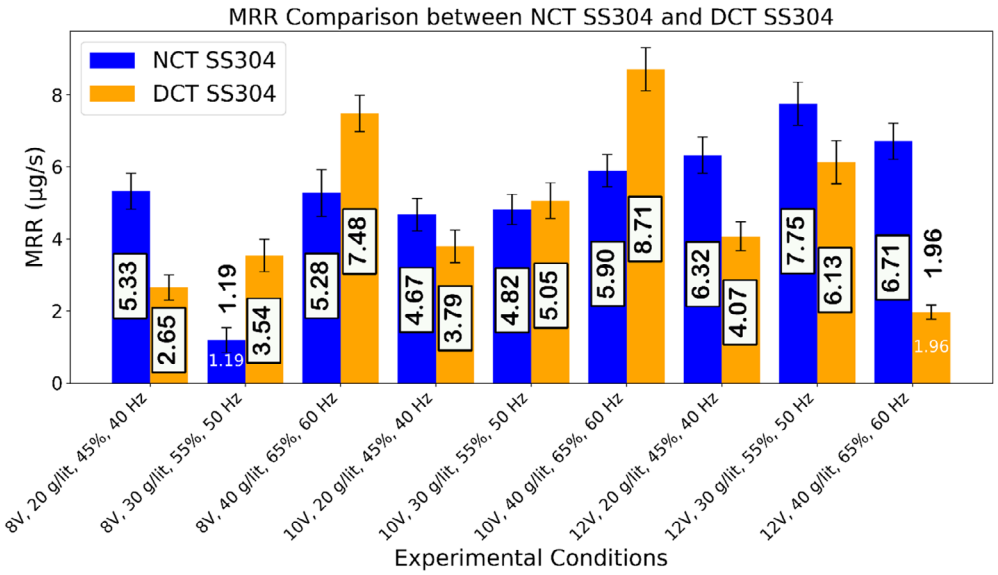

Figure 11. MRR of WAAM SS309 materials using NCT and DCT SS304 electrode during ECM.

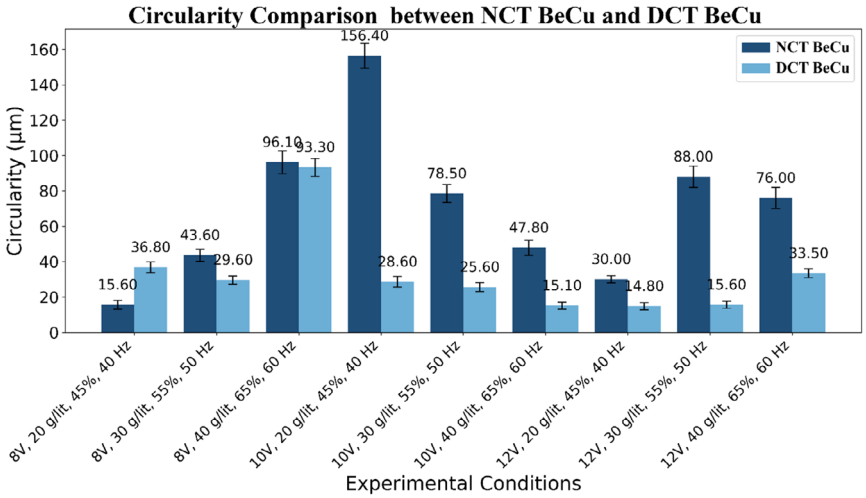

Figure 12. Circularity of WAAM SS309 materials using NCT and DCT BeCu electrode during ECM.

the DCT-treated electrode reduced this to 28.6 µm (**Figure 12**). This decrease in circularity indicates enhanced machining precision, which results from stabilized electrochemical reactions and fewer surface defects on the DCT-treated BeCu electrode. The more stable oxide layer and refined microstructure help decrease dimensional errors during ECM, leading to improved circularity and machining accuracy. These results align with Gautam et al,[49] who observed that cryogenic treatment improves machining performance by enhancing electrochemical stability and dimensional control.

For the SS304 electrode, similar improvements in circularity were observed after DCT. At 10 V, 20 g L^{-1}, 45%, 40 Hz, the untreated SS304 electrode exhibited a high circularity of 198 µm, while the DCT-treated SS304 electrode demonstrated a significant reduction to 13.9 µm (**Figure 13**). This improvement is attributed to the more stable oxide layer formed during DCT, which enhances electrochemical stability and reduces the occurrence of surface defects that contribute to circularity errors. The refined microstructure and improved electrochemical properties help achieve better dimensional control and more precise machining. These findings are consistent with Vora et al.,[50] who reported that cryogenically treated electrodes show improved precision and reduced machining errors due to enhanced electrochemical behavior and a more uniform oxide layer.

The improvements in MRR and circularity for both BeCu and SS304 electrodes after DCT result directly from the enhanced microstructure, better electrical conductivity, and stabilized electrochemical performance. The DCT process refines the grain structure, reduces surface defects, and promotes the formation

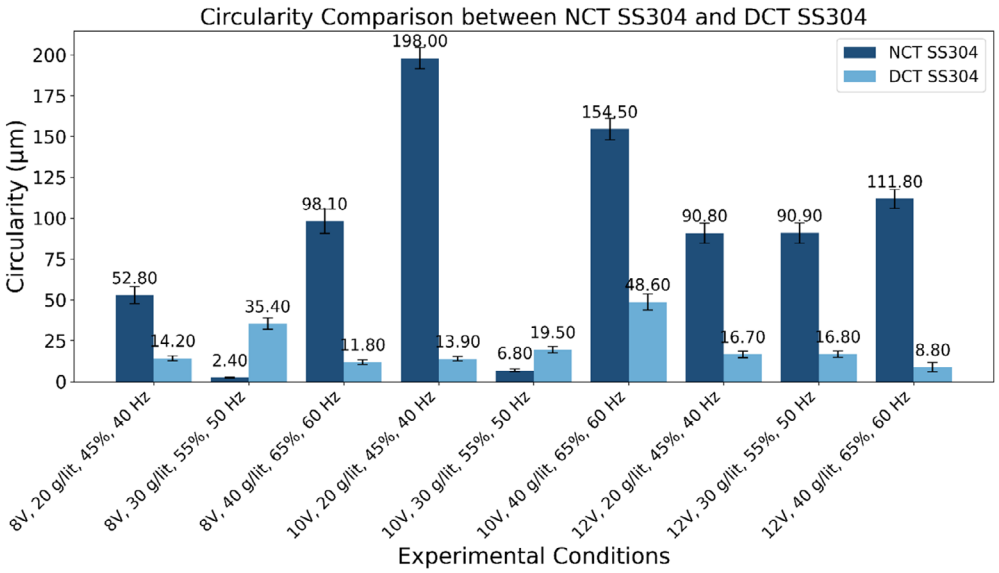

Figure 13. Circularity of WAAM SS309 materials using NCT and DCT SS304 electrode during ECM.

of a more stable oxide layer, all of which contribute to more efficient ECM performance. These results highlight the potential of DCT as an effective method for improving ECM performance, especially in high-precision applications where both high MRR and dimensional accuracy are essential.

Machine Vision Analysis for Circularity: The machine vision analysis of circularity for the machined holes under the 12 V, 40 g L^{-1}, and 60 Hz, 65% duty cycle experimental conditions shows notable differences between the NCT and DCT (cryogenically treated) electrodes for both BeCu and SS304. For the BeCu electrode (**Figure 14**), significant improvements in circularity were observed after DCT. The untreated NCT BeCu electrode showed a circularity of 862.1 µm on the backside (Figure 14a) and 766 µm on the front side (Figure 14c), indicating moderate machining precision. However, after DCT, the circularity increased to 1081.8 µm on the backside (Figure 14b) and 1118.6 µm on the front side (Figure 14d), suggesting that cryogenic treatment improved dimensional accuracy. The increase in circularity for DCT BeCu can be attributed to microstructural refinement and reduced surface defects caused by the DCT process, which stabilizes the electrochemical reaction during ECM, leading to more precise machining and less tool wear.

Similarly, for the SS304 electrode (**Figure 15**), DCT also showed improvements in circularity, although not as significant as those for BeCu. The untreated NCT SS304 electrode had a circularity of 1241.4 µm on the back (Figure 15a) and 1238.4 µm on the front (Figure 15c). After DCT, the circularity improved to 1056.6 µm on the back (Figure 15b) and 1008 µm on the front (Figure 15d). These results suggest that while DCT enhanced the dimensional accuracy of the SS304 electrodes,

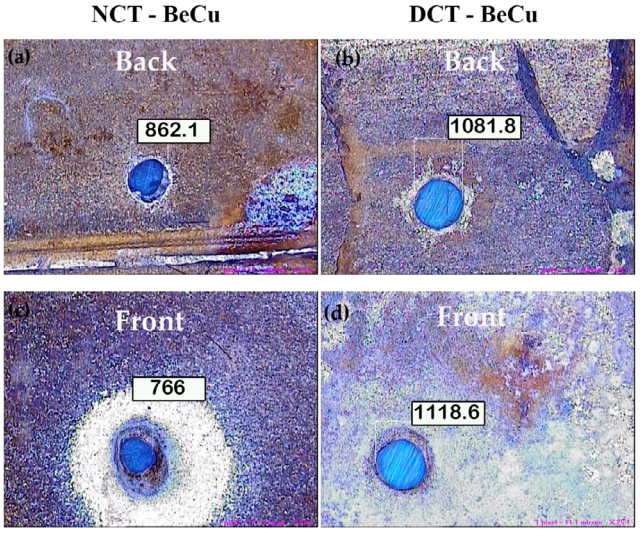

Figure 14. Machine vision analysis of circularity for BeCu electrodes.

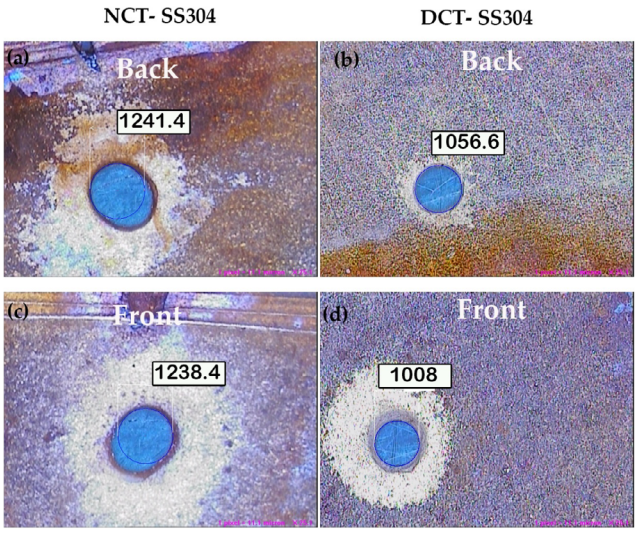

Figure 15. Machine vision analysis of circularity for SS3304 electrodes.

the improvement was less pronounced than for BeCu. This still can be attributed to the refined microstructure and reduced residual stresses in the DCT-treated electrodes, which promote a more stable oxide layer and better electrochemical stability, thereby improving machining performance and reducing surface defects during ECM.

This decrease indicates improvements in machining accuracy, with DCT better able to control hole size and produce uniform-looking holes. Such enhancements align with the results presented by Geethapriyan et al.[51] and Sathish et al.,[52] who have demonstrated that cryogenic treatment enhances electrode performance in ECM by refining microstructures, homogenizing compositions, and increasing electrochemical stability. Overall, the machine vision analysis of circularity clearly demonstrates that cryogenic treatment significantly improves the precision and dimensional accuracy of the machined features in both BeCu and SS304 electrodes. The improved circularity observed for both electrode materials after DCT is a direct result of the refined microstructure, reduced surface defects, and enhanced electrochemical stability. These improvements highlight the potential of DCT-treated electrodes for high-precision ECM applications in industries where dimensional accuracy and surface quality are critical, such as in the aerospace, automotive, and biomedical engineering sectors.

3.6.3. Conicity Behavior of WAAM SS309 Material Using NCT and DCT BeCu and SS304 Electrodes

The conicity observed in ECM machining of WAAM SS309 materials is shown by bar graphs. For the BeCu electrode (**Figure 16**), conicity values are consistently higher with DCT, especially as voltage and electrolyte concentrations increase. These changes are most noticeable at 12 V and 40 g l^{-1} electrolyte concentration, where data were collected at a 60 Hz frequency. At this point, there is a sharp rise in conicity, indicating that tandem DCT provides better cutting stability when longer duty cycles and higher voltages are used.

The BeCu results are consistent with previous research (Sathish et al.,[52]), which found that ECM of metals like stainless steel benefits from increased voltage and electrolyte concentrations, which lead to higher material dissolution rates and improved machining precision. The enhanced conicity in BeCu after DCT suggests that the cryogenic treatment may play a role in refining the electrode surface and improving the dissolution homogeneity, thereby reducing the material's edge erosion and promoting more precise hole shapes.

For SS304 (**Figure 17**), similar trends are observed, although the conicity values are generally lower than those of BeCu. In this case, the conicity drops significantly when the DCT is applied, especially under the same higher voltage and electrolyte concentrations. This decrease in conicity suggests that the DCT-treated SS304 electrode offers a more stable machining environment with less side-erosion. This confirms the material's suitability for achieving more uniform and controlled microhole drilling, aligning with findings from earlier studies on ECM of stainless steel (Sathish et al.,[52]). Overall, these findings validate the effectiveness of DCT in improving the ECM machining performance of both BeCu and SS304 electrodes, especially in terms of conicity control. This aligns with the optimization strategies proposed in the literature, where voltage and duty cycle are shown to significantly affect the conicity and other geometric characteristics of the drilled holes in ECM processes.

3.7. SEM Analysis of NCT BeCu Electrodes in ECM

Figure 18a shows the SEM image of the ECM-machined hole using the untreated BeCu (NCT) electrode on WAAM SS309 material. The surface of the hole exhibits significant roughness and irregular material removal, with visible micropitting around the edges. These imperfections indicate inconsistent electrochemical dissolution during machining, resulting in poor dimensional accuracy. The redeposited debris shown in Figure 18b suggests that the removed material was not effectively evacuated, leading to resolidified material around the hole and contributing to the irregularities. These findings are consistent with previous studies, such as Voglar et al.,[42] which observed similar effects in untreated electrodes during ECM.

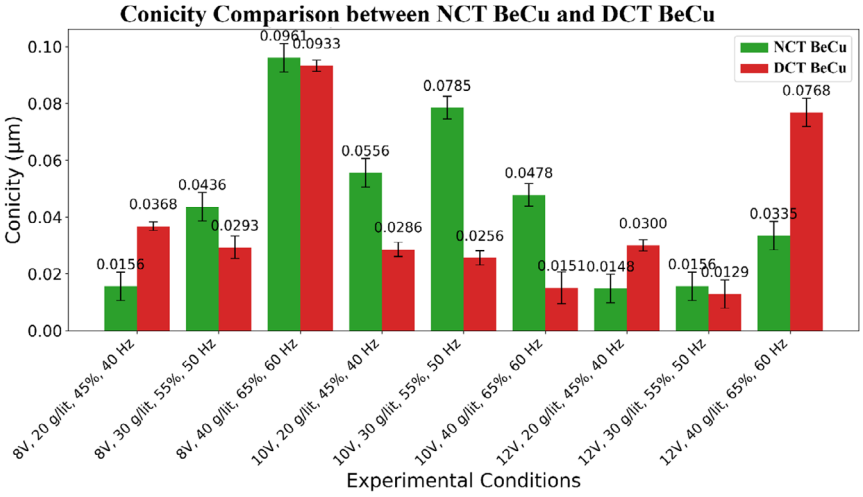

Figure 16. Conicity of WAAM SS309 materials using NCT and DCT BeCu electrode during ECM.

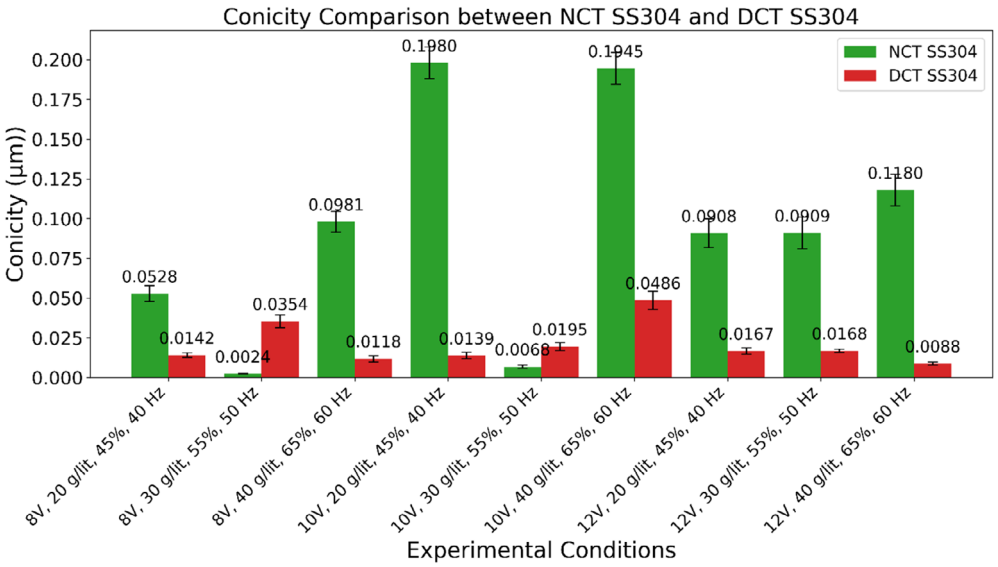

Figure 17. Conicity of WAAM SS309 materials using NCT and DCT SS304 electrode during ECM.

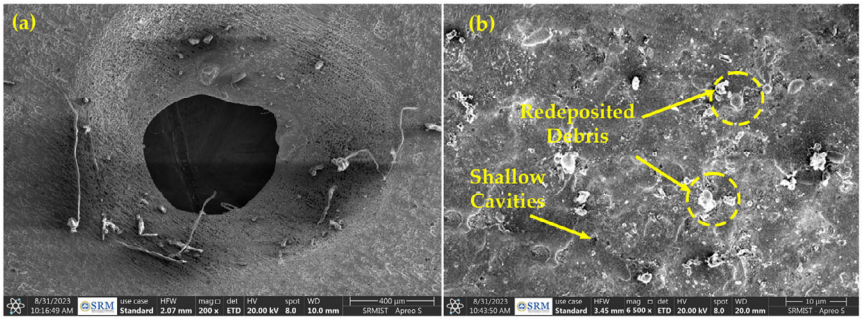

Figure 18. SEM image of the ECM machined hole using the NCT BeCu electrode a) 200x and b) 6500x magnification.

Figure 19 shows the SEM and EDX analysis of the ECM-machined hole using a DCT BeCu electrode on WAAM SS309 material. The SEM image in Figure 19a shows a well-defined, smooth hole with minimal surface roughness. The machining process appears more stable than with the NCT BeCu electrode, with fewer irregularities and a more consistent material removal pattern. This smooth surface is indicative of the improved electrochemical stability provided by the cryogenic treatment. In Figure 19b, the high-magnification SEM image reveals the presence of resolidified debris and a crater formation near the hole's edge. This suggests that, although the machining process is improved, some material was redeposited during the ECM process. This is common when the dissolved material does not evacuate fast enough, leading to redeposition around the machined hole. The crater formation further indicates localized thermal effects at the electrode surface during machining. The EDX spectrum in Figure 19c reveals the chemical composition of the machined surface, with high levels of oxygen (O) and iron (Fe), which are typical of the oxide layer formed during ECM. The presence of chromium (Cr) and nickel (Ni) suggests that the stainless steel composition (SS309) was affected, as expected in the machining process.

These results demonstrate the improvements in machining performance when using DCT-treated BeCu electrodes, featuring more uniform material removal and fewer surface defects compared to untreated electrodes. This aligns with the literature, which indicates that cryogenic treatment enhances the overall performance of ECM electrodes by refining microstructure and boosting electrochemical properties.

3.8. SEM Image of ECM Hole for NCT SS304 Electrode

Figure 20a displays the SEM image of a machined hole made with the NCT SS304 electrode in ECM. The hole has a smooth surface with minor micropitting along the edge. The material removal appears more consistent compared to untreated BeCu electrodes, but there are still signs of irregular dissolution and side erosion. Figure 20b shows the redeposited nanopowder and micropinholes, which occur from incomplete material evacuation during ECM, leading to localized resolidification. These issues indicate that while NCT SS304 offers better stability than

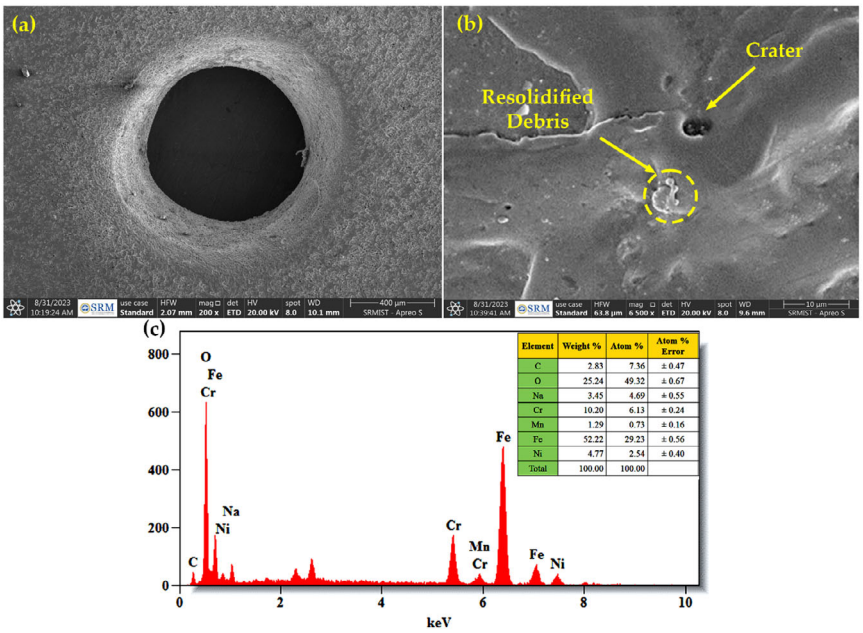

Figure 19. SEM image of the ECM machined hole using the DCT BeCu electrode a) 200x, b) 6500x magnification and c) EDX spectrum.

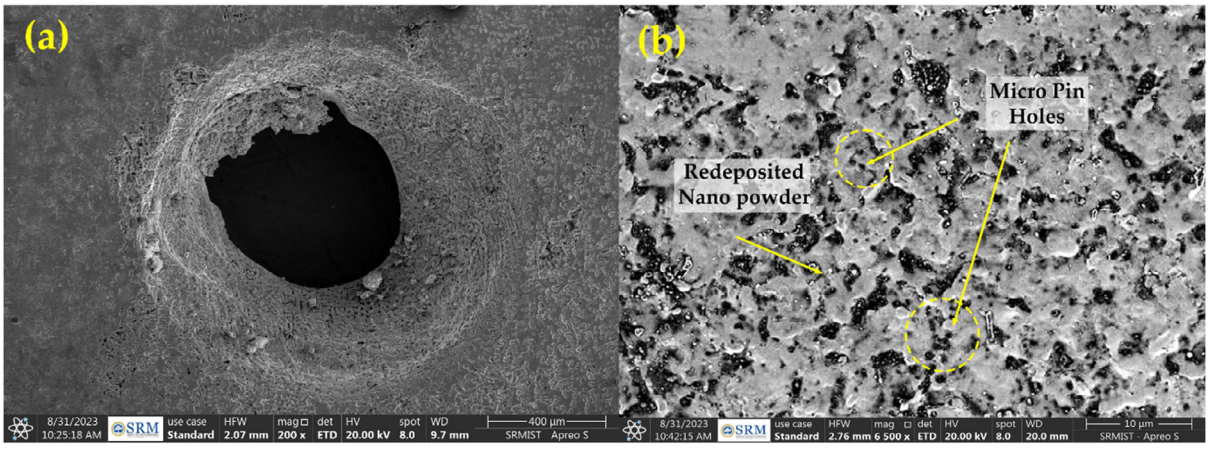

Figure 20. SEM image of the ECM machined hole using the NCT SS304 electrode a) 200x and b) 6500x magnification.

NCT BeCu, it still has less-than-optimal material removal efficiency. This is consistent with previous findings by Geethapriyan et al.,[48] who noted side-erosion and surface roughness as common challenges when using untreated electrodes during ECM.

SEM images of the ECM machined hole on SS304 in (**Figure 21**) show that the SEM analysis provides details about the nature of the machined surface and the formation of resolidified debris, a typical feature associated with the ECM process. The entire surface of the machined area in Figure 21a also appears smooth and clean, which suggests controlled electrochemical dissolution. However, at higher magnification in Figure 21b, resolidified debris and micropitting are observed around the hole, indicating the interaction of material dissolution and redeposition. This phenomenon is typical in ECM when the electrolyte's conductivity causes localized melting of the material, which is then redeposited. Such findings align with Ben Mhahe et al.,[53] who noted that resolidified debris and micropitting result from variations in the MRR during ECM, especially when high-conductivity electrolytes like NaCl and $NaNO_3$ are used.

The EDS spectrum in Figure 21c displays the elemental composition of the machined hole surface, showing a significant presence of oxygen (O) and iron (Fe), which confirms the formation of an oxide layer during the ECM process. The rise in oxygen levels indicates that an oxide film has developed, likely helping to enhance corrosion resistance. The detection of chromium (Cr) and nickel (Ni), typical of SS304, further shows the material's integrity remains intact despite the machining process. The EDS results support previous findings by Voglar et al.,[42] which

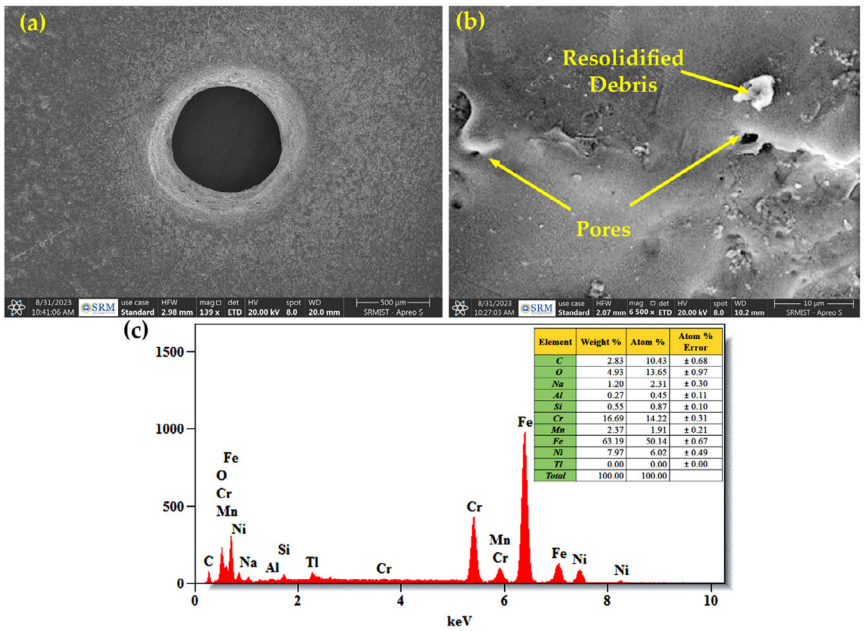

Figure 21. SEM image of the ECM machined hole using the DCT BeCu electrode a) 200x, b) 6500x magnification and c) EDX spectrum.

showed that the ECM process leads to oxide formation on stainless steel surfaces, enhancing stability and passivation. Pore holes on the machined surface indicate that unstable electrochemical dissolution also contributes to the results reported by Vora et al.,[54] who observed similar surface defects when ECM was performed with less passivated electrodes or stronger mobilized electrolytes.

4. Conclusions

This study examines the effects of DCT on BeCu and SS304 electrodes during ECM of WAAM SS309. The findings reveal notable improvements in both machining performance and electrode properties following DCT. Specifically, SS304 electrodes showed an 83.31% increase in electrical conductivity, which enhances ion transfer during ECM. This boost was associated with a refined microstructure, leading to higher MRRs, with SS304 reaching a peak MRR of 8.71 $\mu g\,s^{-1}$ compared to 5.90 $\mu g\,s^{-1}$ for NCT SS304. The BeCu electrodes also experienced a significant rise in MRR, achieving a peak of 8.56 $\mu g\,s^{-1}$ under similar conditions.

Along with the improvements in MRR, DCT greatly increased the corrosion resistance of both electrodes. The corrosion current density for BeCu dropped by 26.1%, and for SS304, it decreased by 43.5%, showing a lower chance of corrosion. This boost in corrosion resistance is due to the formation of a more stable oxide layer, which enhances electrochemical stability. The shift toward more positive corrosion potentials and the lower current responses seen in the electrochemical tests also support the improved stability of the DCT-treated electrodes.

SEM and EDX analysis further confirmed that DCT-treated electrodes exhibited smoother surfaces, fewer defects, and less resolidified debris compared to their untreated counterparts. These findings support the hypothesis that DCT reduces surface roughness and enhances microstructural integrity, leading to improved machining accuracy. The circularity of the machined features also improved significantly, with SS304 showing a decrease in circularity error from 198 to 13.9 µm and BeCu from 156.4 to 28.6 µm after DCT, indicating better dimensional accuracy during ECM. The combined improvements in electrochemical stability, corrosion resistance, microstructure, and machining precision suggest that DCT-treated SS304 electrodes are particularly suitable for high-precision ECM of WAAM SS309. These enhancements make DCT-treated electrodes ideal for industries where high MRR, improved dimensional control, and minimal tool wear are critical, such as aerospace, automotive, and biomedical engineering. Future studies should focus on optimizing electrolyte compositions and evaluating the long-term performance of DCT-treated electrodes under more demanding ECM conditions.

Acknowledgements

The authors declare that no funding was received for the research, authorship, or publication of this article.

Conflict of Interest

The authors declare no conflict of interest.

Author Contributions

Karunakaran Kuppusamy: research administration. **Gopi Periyappillai**: testing and validation. **Saravanakumar Sengottaiyan**: investigation and writing original draft. **Periyasamy Rajendran**: resources and experimental works.

Data Availability Statement

The data supporting the findings of this study are available within the article. No additional datasets were generated or analyzed during the current study.

Keywords

corrosion resistance, deep-cryogenic treatment, electrochemical machining, material removal rate, wire arc additive manufacturing

Received: October 13, 2025
Revised: December 3, 2025
Published online:

[1] E. Uhlmann, M. Polte, S. Yabroudi, *Procedia CIRP* **2022**, *113*, 611.
[2] A. Nair, W. Bizoń, S. Skoczypiec, R. Bogucki, L. Selvarajan, *J. Braz. Soc. Mech. Sci. Eng.* **2024**, *46*, 673.
[3] R. L. Lin, W. Y. Li, L. Li, C. J. Liao, *Adv. Eng. Mater.* **2024**, *26*, 2302083.
[4] M. F. Saffiudeen, V. Swaminathan, F. T. Mohammed, A. Syed, Y. A. Alamri, M. N. Al Qahtani, *Arabian J. Sci. Eng.* **2024**, *50*, 13887.
[5] M. F. Wang, C. Liu, G. Y. Bai, H. Y. Liu, Y. B. Liu, D. X. Fan, Z. X. Wang, G. B. Pang, *Vacuum* **2025**, *240*, 114487.
[6] D. Janardhanan, H. Perianna, *Int. J. Adv. Manuf. Technol.* **2024**, *130*, 3819.
[7] A. Sinha, P. S. Rao, M. Y. Khan, G. Singh, *Mater. Today Proc.* **2023**.
[8] A. B. Pawar, S. S. Chavan, P. V. Jadhav, D. B. Jadhav, *Eng. Res. Express* **2025**, *7*, 035523.
[9] M. Frensemeier, D. Schirra, M. Weinmann, O. Weber, E. Kroner, *Adv. Eng. Mater.* **2016**, *18*, 1388.
[10] S. Madhankumar, S. Rajesh, R. Balamurugan, N. T. S. Ram, S. Venuprasath, S. T. Ahamed, *IOP Conf. Ser. Mater. Sci. Eng.* **2021**, *1059*, 012008.
[11] R. K. Upadhyay, A. K. Chakraborty, S. S. Majhi, A. C. Singh, B. Kumar, N. Yadav, *Surf. Sci. Technol.* **2025**, *3*, 11.
[12] A. Gomez-Gallegos, F. Mill, A. R. Mount, S. Duffield, A. Sherlock, *Int. J. Adv. Manuf. Technol.* **2018**, *95*, 2959.
[13] S. I. Vasilevskaya, E. D. Golovin, N. V. Stepanova, *Mach. Sci. Technol.* **2025**, *29*, 488.
[14] M. M. Maktuf, R. R. Shwaish, S. H. Aghdeab, *BIO Web Conf.* **2024**, *97*, 00034.
[15] A. E. K. Mohammad, D. Wang, *Int. J. Adv. Manuf. Technol.* **2016**, *86*, 1909.
[16] P. Nanou, A. Zarkadoulas, P. K. Pandis, I. Tsilikas, I. Katis, D. Almpani, N. Orfanoudakis, N. Vourdas, V. Stathopoulos, *Int. J. Adv. Manuf. Technol.* **2024**, *133*, 307.
[17] Y. Zhang, Y. Fang, C. Zhang, *Int. J. Adv. Manuf. Technol.* **2025**, *137*, 2181.
[18] R. Venkatesh, A. Sharma, K. Karthik, R. Kumar, P. K. K. Vivekananda, M. Vinayagam, M. E. M. Soudagar, S. Al Obaid, S. A. Alharbi, *Int. J. Met.* **2025**, *19*, 3316.
[19] A. Hannan, S. Mehmood, M. A. Ali, M. H. Raza, M. U. Farooq, S. Anwar, A. A. Adediran, *Sci. Rep.* **2024**, *14*, 28930.
[20] K. Ishfaq, M. Sana, M. U. Waseem, M. A. Mahmood, S. Anwar, *Int. J. Adv. Manuf. Technol.* **2024**, *134*, 5951.
[21] S. Karthikeyan, S. Kathiresan, T. Suja, *J. Mater. Eng. Perform.* **2025**, *34*, 12861.
[22] Ş. Baysal, F. H. Çakir, F. Ceritbinmez, E. Kanca, *Can. Metall. Q.* **2025**, *4433*, pp. 1–12.
[23] N. Manikandan, M. Arumugam, *J. Mater. Eng. Perform.* **2024**, *34*, 4853.
[24] S. Saravanan, S. Sengottaiyan, R. Aravind, S. Krishnakumar, *J. Mater. Eng. Perform.* **2025**.
[25] G. Çam, A. Günen, *J. Magnesium Alloys* **2024**, *12*, 1663.
[26] M. Srivastava, S. Rathee, A. Tiwari, M. Dongre, *Mater. Chem. Phys.* **2023**, *294*, 126988.
[27] M. Thirukumaran, S. R. Stalin, M. M. Simon, R. Senthilkumar, S. Bhuvanesh, K. Senthilkumar, *Int. J. Interact. Des. Manuf.* **2025**.
[28] K. Srividya, S. Ravichandran, M. Thirunavukkarasu, I. Veeranjaneyulu, P. Satishkumar, K. Bharadwaja, N. S. Rao, R. Subbiah, J. E. Manikanta, *Int. J. Interact. Des. Manuf.* **2024**, *18*, 1459.
[29] Z. Xu, Z. Huang, Y. Wang, C. Lin, X. Xu, *J. Mater. Eng. Perform.* **2021**, *30*, 7542.
[30] S. Dong, Z. Wang, Y. Wang, *Int. J. Adv. Manuf. Technol.* **2017**, *88*, 827.
[31] S. Dong, Z. Wang, Y. Wang, *Int. J. Adv. Manuf. Technol.* **2017**, *93*, 857.
[32] I. M. Rashedul, Y. Zhang, K. Zhou, G. Wang, T. Xi, L. Ji, *Micromachines* **2021**, *12*, 1077.
[33] G. Liu, Z. Gong, Y. Yang, J. Shi, Y. Liu, X. Dou, C. Li, *Electrochem. Commun.* **2024**, *160*, 107677.
[34] S. S. Gill, H. Singh, R. Singh, J. Singh, *Int. J. Adv. Manuf. Technol.* **2010**, *48*, 175.
[35] S. T. Prabakaran, S. Sengottaiyan, D. Yogaraj, V. S. Shaisundaram, *J. Mater. Eng. Perform.* **2025**.
[36] M.-K. Ji, M.-S. Lee, Y.-T. Hyun, T.-S. Jun, *Mater. Today Commun.* **2023**, *36*, 106514.
[37] S. Arumugam, V. Elumalai, L. Thangavelu, G. Thangamani, *Multiscale Multidiscip. Model. Exp. Des.* **2025**, *8*, 344.
[38] B. Ghoshal, B. Bhattacharyya, *Int. J. Adv. Manuf. Technol.* **2015**, *76*, 39.
[39] G. Periyappillai, S. Subbarayan, S. Sengottaiyan, *Mater. Chem. Phys.* **2025**, *333*, 130175.
[40] S. Saravanakumar, S. Sathiyamurthy, V. Vinoth, *Meas. J. Int. Meas. Confed.* **2024**, *235*, 114912.
[41] N. Arivazhagan, M. Manikandan, G. Kumar, *Heliyon* **2024**, *10*, e35279.
[42] J. Voglar, Novak, P. Jovičević-Klug, B. Podgornik, T. Kosec, *Metals* **2021**, *11*, 14.
[43] S. Sengottaiyan, V. S. Shaisundaram, M. S. Basha, B. Deepanraj, N. Senthilkumar, *Results Eng.* **2025**, *26*, 104818.
[44] S. Ramesh, B. Bhuvaneshwari, G. S. Palani, D. Mohan Lal, K. Mondal, R. K. Gupta, *Vacuum* **2019**, *159*, 468.
[45] S. S. Gill, J. Singh, *Mater. Manuf. Process.* **2010**, *25*, 378.
[46] P. Suresh, S. Kumaravel, S. Sengottaiyan, P. Muthukumar, *Compos. Interfaces* **2025**, *00*.
[47] V. S. Jatti, R. B. Dhabale, A. Mishra, N. K. Khedkar, V. S. Jatti, A. V. Jatti, *Appl. Syst. Innovation* **2022**, *5*, 112.
[48] G. Thangamani, M. Thangaraj, K. Moiduddin, H. Alkhalefah, S. Mahalingam, P. Karmiris-Obratański, *Materials* **2022**, *15*, 4831.
[49] N. Gautam, A. Goyal, S. S. Sharma, A. D. Oza, R. Kumar, *Mater. Today Proc.* **2022**, *57*, 615.
[50] J. Vora, H. Parmar, R. Chaudhari, S. Khanna, M. Doshi, V. Patel, *J. Mater. Res. Technol.* **2022**, *20*, 2748.
[51] G. Thangamani, M. Thangaraj, K. Moiduddin, S. H. Mian, H. Alkhalefah, U. Umer, *Metals* **2021**, *11*, 247.
[52] T. Sathish, *J. Mater. Res. Technol.* **2019**, *8*, 4354.
[53] F. Ben Mhahe, Y. Zhang, C. Chen, W. I. Umoren, *Int. J. Electrochem. Sci.* **2024**, *19*, 100647.
[54] J. Vora, R. Pandey, P. Dodiya, V. Patel, S. Khanna, V. Vaghasia, R. Chaudhari, *Materials* **2023**, *16*, 5147.
[55] B. Mouliprasanth, P. Hariharan, *Exp. Tech.* **2020**, *44*, 259.
[56] G. Thangamani, S. K. Tamang, S. S. Rajput, P. Kumar, G. Kumarasamy, *J. Appl. Electrochem.* **2025**, *55*, 1455.
[57] N. Pradeep, K. S. Sundaram, M. P. Kumar, *J. Braz. Soc. Mech. Sci. Eng.* **2019**, *41*, 323.

[58] M. S. Park, C. N. Chu, *J. Micromech. Microeng.* **2007**, *17*, 1451.
[59] L. Zhu, J. Hao, B. Xu, B. Wang, *Int. J. Adv. Manuf. Technol.* **2022**, *121*, 6049.
[60] J. R. K. V. Kumaar, R. Thanigaivelan, M. Soundarrajan, *Chem. Ind. Chem. Eng. Q.* **2022**, *28*, 329.
[61] E. Nas, N. A. Özbek, *Surf. Rev. Lett.* **2020**, *27*, 1950177.
[62] E. Nas, *Tribol. Int.* **2024**, *193*, 109453.